Supporting information for: Charge carrier motion in disordered conjugated polymers: a multiscale ab-initio study

Nenad Vukmirović,* and Lin-Wang Wang

Computational Research Division, Lawrence Berkeley National Laboratory, Berkeley, CA 94720, USA.

E-mail: NVukmirovic@lbl.gov

1 Charge density motif generation

The rationale behind the use of charge density motifs in the so called charge patching method (CPM) comes from the observation that in semiconducting systems the charge density around a given atom depends mainly on its local environment. The motifs corresponding to equilibrium bond lengths and angles were generated from a charge density calculated using DFT in local density approximation (LDA) (the code PEtot[1] with norm conserving pseudopotentials with kinetic energy cutoff of 60 Ry was used) of small prototype systems in a manner previously described.[2] Three unit long oligomers of hexyl-thiophene were used as prototype systems for motif generation. To properly describe the changes in the atom environment, the so called derivative motifs were introduced which describe the change of the charge density motif due to a particular bond length perturbation or due to change of a certain angle in the system. Special care is taken to avoid any double counting, which might take place especially in systems with rings where bond lengths

and angles satisfy certain constraints. We find that the derivative motifs are especially important for a correct description of electron-phonon coupling.

2 Generation of the atomic structure

The details of the procedure are essentially the same as in the previous publication[3] and we only briefly outline it here. The CFF91 force field,[4,5] modified to properly account for torsion potentials that mainly determine the shape of the chains, was used. The MD simulation was performed using the LAMMPS code.[6,7] Five P3HT chains, each 20 units long, (containing 2510 atoms alltogether) are initially placed in a large cubic box at a high temperature. The size of the box is then gradually decreased down to 29.286 Å, corresponding to the experimental density of P3HT of 1.1 $\mathrm{g/cm^3}$.[8–11] Subsequently, the system was cooled down to room temperature and relaxed to a local minimum.

3 Calculation of wave functions and energies

The charge density $\rho(\mathbf{r})$ is calculated by simply adding the precalculated nonspherical charge density motifs assigned to each of the atoms. After the charge density is obtained, one needs to solve the single-particle Kohn-Sham equation

$$\left(-\frac{\hbar^2}{2m_0}\nabla^2 + V_{\mathrm{ion}} + V_{\mathrm{H}} + V_{\mathrm{XC}}\right)\psi_i(\mathbf{r}) = \varepsilon_i\psi_i(\mathbf{r}). \tag{1}$$

to obtain the wave functions $\psi_i(\mathbf{r})$ and energies ε_i of single-particle states. In Eq. 1 V_{ion} is the (nonlocal) potential of ions and core electrons modeled using Troullier Martins norm conserving pseudopotentials. V_{H} is the Hartree potential of electrons given as

$$V_{\mathrm{H}}(\mathbf{r}) = \frac{1}{4\pi\varepsilon_0}\int \mathrm{d}\mathbf{r}'\frac{\rho(\mathbf{r}')}{|\mathbf{r}-\mathbf{r}'|}, \tag{2}$$

$V_{\mathrm{XC}}(\mathbf{r})$ is the exchange-correlation potential, which is in LDA a well-known function of charge density $\rho(\mathbf{r})$ at the same point $\mathbf{r}$. Therefore, knowing the charge density, one straight-forwardly constructs the single particle Hamiltonian

$$H = \left(-\frac{\hbar^2}{2m_0}\nabla^2 + V_{\mathrm{ion}} + V_{\mathrm{H}} + V_{\mathrm{XC}} \right). \tag{3}$$

One can therefore think of the CPM also as the method for constructing the single-particle Hamiltonian and not only the charge density.

The Kohn-Sham equation 1 for the several top states in the valence band is then solved using the folded spectrum method,[12] as implemented in the ESCAN code.[13] We solve for the 16 top states in the valence band.

It should be particularly emphasized that the calculation of the electronic structure using the charge patching method yields the results of the same accuracy as the DFT in LDA (with the differences in eigenenergies of the order of tens of meV only), as we have demonstrated for the case of polythiophenes and many other organic systems in our recent publications.[2,3]

4 Calculation of phonon spectrum and electron-phonon coupling

The phonon spectrum is modeled using the same classical force field used in MD simulations. The energies and eigenvectors of all phonon modes are calculated by diagonalizing the dynamical matrix defined as

$$K_{rs,pq} = \frac{1}{\sqrt{m_r m_p}} \frac{\partial^2 E}{\partial x_{rs} \partial x_{pq}}, \tag{4}$$

where E is the force field energy, m_r the mass of the r-th atom and x_{rs} its s-th coordinate ($s \in \{1,2,3\}$). Angular frequency ω_μ of phonon mode μ is given as the square root of the eigenvalue

of the dynamical matrix

$$\sum_{pq} K_{rs,pq} R_{pq}^{(\mu)} = \omega_\mu^2 R_{rs}^{(\mu)} \tag{5}$$

and the normal coordinate of mode μ is given as

$$v_\mu = \sum_{rs} R_{rs}^{(\mu)} (x_{rs} - x_{rs}^0) \sqrt{m_r}, \tag{6}$$

where $(x_{rs} - x_{rs}^0)$ is the s-th coordinate of the displacement of atom r from its equilibrium position. The transition rate from the electronic state i to j due to interaction with phonons is given by the Fermi Golden rule expression

$$W_{ij} = \pi \sum_\mu \frac{\left|\mathscr{M}_{ij,\mu}\right|^2}{\omega_\mu} \left[\left(N_\mu + 1\right) \delta\left(\varepsilon_i - \varepsilon_j - \hbar\omega_\mu\right) + N_\mu \delta\left(\varepsilon_i - \varepsilon_j + \hbar\omega_\mu\right) \right], \tag{7}$$

where N_μ is the phonon occupation number of mode μ given by the Bose-Einstein distribution at temperature T, ε_i the single particle energy of state i and

$$\mathscr{M}_{ij,\mu} = \left\langle \psi_i \left| \frac{\partial H}{\partial v_\mu} \right| \psi_j \right\rangle \tag{8}$$

the electron-phonon coupling matrix element between electronic states i and j (obtained as solutions ψ_i and ψ_j of Eq. 1 in a way described in the previous section of this Supporting information) due to phonon mode μ. H is the single particle Hamiltonian defined in Eq. 3.

To calculate the change $\partial H/\partial v_\mu$ of the single particle Hamiltonian due to atom displacements of the phonon mode μ, it is sufficient to calculate the changes due to displacement of each of the atomic coordinates $\partial H/\partial x_{rs}$ and then perform a transformation making use of the equation (6). $\partial H/\partial x_{rs}$ can be found by constructing the single-particle Hamiltonian for the initial atomic structure (as described in the previous section of this Supporting information) and the atomic structure where atom r is displaced by a small Δx_{rs} in the direction s. We note that the CPM is particularly suitable for the computationally efficient construction of these Hamiltonian perturbations $\partial H/\partial x_{rs}$ since the only difference in the charge density of the perturbed and initial system comes from the

charge density motifs of the atom that is displaced and its neighbors. Therefore, the charge density of the perturbed system can be found simply by adding the above difference to the charge density of the original system (i.e. one does not have to calculate it from the beginning).

With ψ_i, ψ_j and $\partial H/\partial v_\mu$ at hand, we calculate $\mathscr{M}_{ij,\mu}$ straightforwardly from its definition (Eq. 8). Technically, this is done first by acting on ψ_j with operator $\partial H/\partial v_\mu$ (using one of the procedures in the ESCAN code[13]) and then simply calculating the scalar product of the obtained vector with ψ_i.

By comparing the results obtained by the described procedure and direct DFT/LDA calculations for the similar but smaller ($\sim$300 atom) systems, we found that the difference in Hamiltonian perturbation $\partial H/\partial v_\mu$ obtained by the two methods is of the order of 10 %. These tests were performed as follows. The test system chosen consists of 3 chains of polythiophene, each containing 15 rings, which makes 321 atoms alltogether and therefore it is still computationally feasible to do (a limited number of) DFT calculations on such a system. The atomic structure of this system was generated from classical MD using a simulated annealing procedure, in a similar manner as described in Sec. 2 of this Supporting information, which makes this system disordered and very similar to the larger 2510 atom P3HT system which is the main subject of this work. We have performed 22 tests (labeled as T1-T22) as follows. The tests were performed by first constructing the single-particle Hamiltonian H_{CPM} in a way described in Sec. 3, i.e. starting from charge density $\rho_{\mathrm{CPM}}(\mathbf{r})$ obtained from charge patching. In tests T1-T19 the atoms are then displaced according to phonon mode μ (the energies of the phonon modes in tests T1-T19 that span the entire spectrum where there are phonon modes is reported in Table 1, while the displacements are normalized such that the largest one is 0.002 Å) and the new single particle Hamiltonian H'_{CPM} is constructed in the same way that H_{CPM} was constructed. The Hamiltonian perturbation is then obtained simply as $P_{\mathrm{CPM}} = H'_{\mathrm{CPM}} - H_{\mathrm{CPM}}$. The same steps are then repeated with a difference that one starts with charge density $\rho_{\mathrm{DFT}}(\mathbf{r})$ obtained from direct self-consistent DFT calculations and therefore obtains H_{DFT}, H'_{DFT} and $P_{\mathrm{DFT}} = H'_{\mathrm{DFT}} - H_{\mathrm{DFT}}$. The contribution to P-operators comes only from the V_{H}, V_{XC} and V_{ion} in Eq. 3, since the kinetic energy term does not change. We compare the local parts

of P_{CPM} and P_{DFT} (which we call $P^{\mathrm{LOC}}_{\mathrm{CPM}}(\mathbf{r})$ and $P^{\mathrm{LOC}}_{\mathrm{CPM}}(\mathbf{r})$), since the nonlocal part (that originates from V_{ion} in Eq. 3) is the same in both cases. We quantify the difference between $P^{\mathrm{LOC}}_{\mathrm{CPM}}(\mathbf{r})$ and $P^{\mathrm{LOC}}_{\mathrm{DFT}}(\mathbf{r})$ as

$$\beta = \frac{\int \left| P^{\mathrm{LOC}}_{\mathrm{CPM}}(\mathbf{r}) - P^{\mathrm{LOC}}_{\mathrm{DFT}}(\mathbf{r}) \right| \mathrm{d}\mathbf{r}}{\int \left| P^{\mathrm{LOC}}_{\mathrm{DFT}}(\mathbf{r}) \right| \mathrm{d}\mathbf{r}} \times 100\% \tag{9}$$

The results obtained for the difference β are presented in Table 1.

Table 1: The comparison of Hamiltonian perturbations obtained from DFT/LDA and CPM

test label	$\hbar\omega_\mu$ (meV)	β
T1	10	8.9%
T2	20	8.3%
T3	30	7.4%
T4	40	8.0%
T5	50	10.3%
T6	80	9.3%
T7	90	8.9%
T8	100	8.3%
T9	110	11.1%
T10	120	8.8%
T11	130	12.1%
T12	140	10.5%
T13	160	13.0%
T14	170	12.8%
T15	180	9.9%
T16	190	9.2%
T17	200	8.7%
T18	210	10.7%
T19	390	10.5%

test label	β
T20	8.3%
T21	7.9%
T22	8.0%

We further performed the tests (that we label as T20-T22) where we displace atoms not according to a particular phonon mode, but randomly (the displacement of each atom in each direction is drawn from a uniform distribution from the interval -0.002 Åto 0.002 Å). We believe that the error β obtained in such tests T20-T22 should be similar to a typical average β for all phonon modes. From all the results presented in Table 1 one can conclude that the accuracy of the CPM calculated

Hamiltonian perturbations is of the order of 10%.

In Figure 1, we present the histogram of the appearance of different values of the dimensionless electron-phonon coupling constant $g_{ij,\mu}$, related to $\mathscr{M}_{ij,\mu}$ via $g_{ij,\mu} = \mathscr{M}_{ij,\mu} \frac{1}{\hbar\omega_\mu} \sqrt{\frac{\hbar}{2\omega_\mu}}$. The histogram includes $g_{ij,\mu}$ among all calculated electronic states and all phonon modes, for one realization of the system at the L_2 length scale. One can note that practically all $g_{ij,\mu}$ are significantly smaller than 1, which suggests weak coupling among most of the states and therefore gives a first indication that the use of Eq. 7 based on first order perturbation theory is valid. From Figure 1 one can also see that there are few coupling constants which are of the order of 1, for which the use of perturbation theory does not give the transition rates which are quantitatively correct. We however expect that these transition rates have a very weak influence on the overall transport (since there are just a few of them). In what follows we provide two numerical proofs of such an expectation.

1) We repeat the whole mobility calculation, where we set all dimensionless coupling constants which are larger than 0.1 to zero. The comparison of such a calculation with the previous calculation where coupling constants were not changed gives an insight into the influence of coupling constants larger than 0.1 on mobility of the system. Such a comparison is given in Figure 2 and shows that the coupling constants larger than 0.1 affect the mobility by less than 5%.

2) In Figure 3 we show the histogram of contributions of different values of dimensionless coupling constants to the current. The histogram was obtained in a similar manner as histograms shown in Figs. 4b and 4d of the main paper. A certain reference plane is chosen and each transition rate that contributes to current through that plane was decomposed into contributions from individual coupling constants in Eq. 7. In such a way the contribution of each coupling constant to the current is identified. The histogram is then formed by adding the contributions of coupling constants that fall into specified range of their values. The final histogram is obtained by averaging such histograms for different reference planes. The histogram presented in Figure 3 shows that the contribution to current of coupling constants of the order of one is very small.

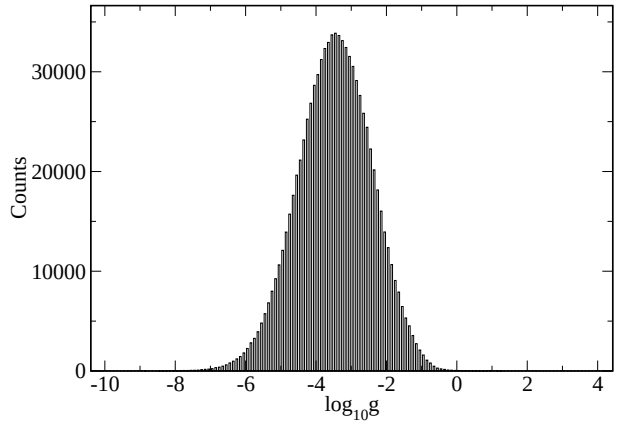

Figure 1: The histogram of appearance of different values of dimensionless electron-phonon coupling constant $g_{ij,\mu}$ for one realization of the system at the L_2 length scale.

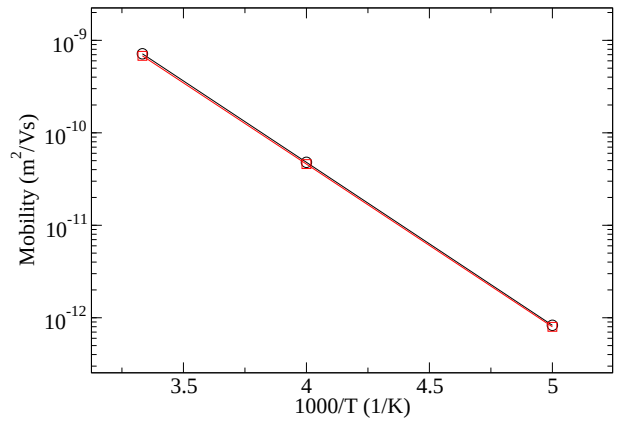

Figure 2: The comparison of the mobility calculation where all dimensionless coupling constants less than 0.1 where set to zero (squares) and the original mobility calculation where these constants were not changed (circles).

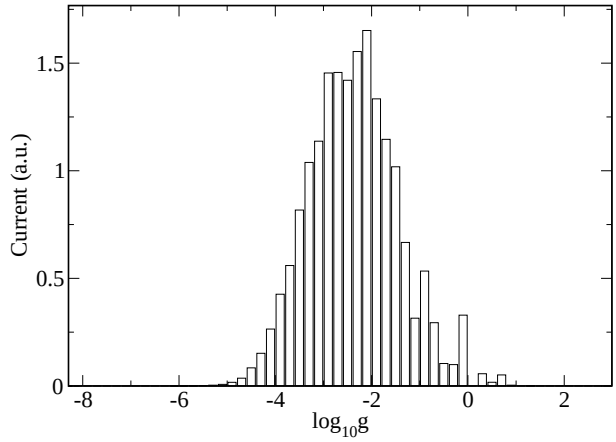

Figure 3: The histogram of contributions of different dimensionless coupling constants $g_{ij,\mu}$ to the current.

5 The role of polarons

Recent density functional theory calculations [14,15] have shown that polaron binding energy in long straight polythiophene chains is of the order of few meVs only. It is on the other hand not clear whether the same is the case for the state localized on a part of the long disordered chain, i.e. whether polaron binding energy is mainly determined by the degree of wavefunction localization or by the length of the whole chain. To gain insight into this problem, we have performed DFT calculations of polaron binding energy for the VBM state of a 10 unit long chain whose shape is shown in Figure 4. The chain is disordered except for the four central units which are on the straight line and the wavefunction is localized there. The calculation was performed using the NWChem code. [16] Polaron binding energy was calculated as the difference between the total energy of the singly charged chain in the atomic configuration of the neutral chain and the total energy of the fully relaxed singly charged chain. Interring torsion angles are kept fixed in order to preserve the shape of the chain, while all other coordinates are allowed to relax. This is a simplified model keeps the overall shape of the chain unchanged (no torsion angle change) to mimic the effects of interlocking neghboring polymer chains in a real disordered system. Thus, in a real system, allowing the torsion angles to relax might increase the polaron binding energy to some extent.

6-31G basis set was used and LDA or B3LYP density functionals were used. The results for the disordered chain were compared to the results for straight chains, either 4 or 10 units long and are presented in Table 2. Polaron binding energy of the disordered chain is closer to the polaron binding energy of the 10 unit straight chain than to the one of the 4 units long straight chain, which suggests that its value is largely determined by the total chain length. Therefore, one can conclude that polaron binding energy of a carrier localized on k units of a long disordered chain is significantly reduced in comparison to the one of the k units long molecule.

Table 2: Polaron binding energies of polythiophene chains calculated using DFT

	disordered chain	10 unit straight chain	4 unit straight chain
LDA	62.8 meV	46.1 meV	89.2 meV
B3LYP	107.5 meV	84.6 meV	138.7 meV

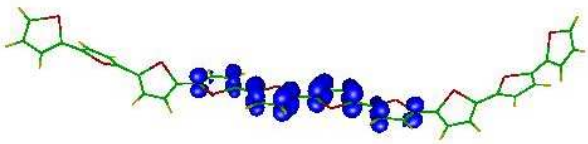

Figure 4: The 10 units long disordered polythiophene chain and its VBM wavefunction.

6 The role of broadening of the delta function

Within all the calculations performed, the delta function in the Fermi's Golden rule expression was replaced by a Gaussian with standard deviation of 10 meV. Since the phonon density of states is continuous one does not expect that the transition rates and consequently the mobility would heavily depend on the choice of this parameter. To check for this, the mobility at several temperatures and for the several values of the broadening parameter was calculated. The results are shown in Figure 5, indicating that our expectations were correct, since the mobility changes by less than 30% when broadening parameter is changed from the one used (10 meV) within the reasonable limits (increased or decreased within a factor of 2).

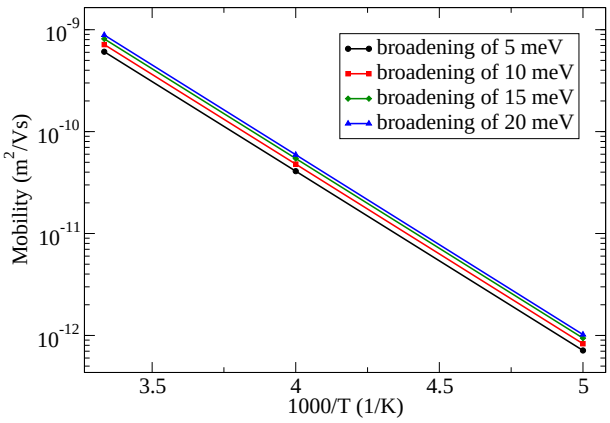

Figure 5: The mobility of the system for several different values of the broadening parameter.

7 Convergence check

One has to check that $m_1 = 10$ numerical samples at length scale L_2 is sufficient to get convergent statistical results for the mobility. The results obtained when smaller number of samples was taken are presented in Figure 6 and demonstrate that the results obtained with $m_1 = 10$ are convergent.

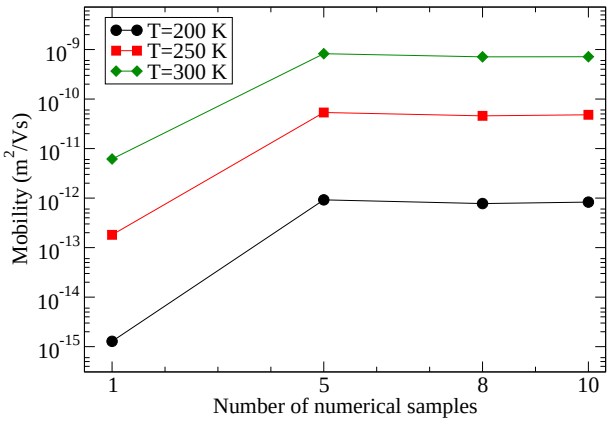

Figure 6: The dependence of the mobility on the number of numerical samples m_1 used to build the conductor network.

8 The procedure for calculating the electron-phonon coupling elements of the states from neighboring boxes

The electron-phonon coupling matrix elements between states from the same box are available from the calculation at length scale L_2. However, the matrix elements between states from neighboring boxes are not available. An approximation needs to be introduced to calculate them as well. First of all, only the transitions between the states from a certain box and its 26 neighbors (by neighbors we consider the boxes that have a common side or a common edge or a common corner with the given box) are considered. The coupling element between state i in box b_i and state j in box b_j is calculated as is now described. The distances from the state i to all other states in box b_i and neighboring boxes are calculated and sorted in ascending order. Let the state j be the $k-$th state in this array. A periodic system filled with the same samples as box b_i is considered then. The states in box b_i and its neighboring boxes in this system are also sorted according to the distance from state i and the state which is the $k-$th is identified. Let's call this state j'. The matrix element of the coupling between i and j' is available from the calculation on length scale L_2 for the sample that fills the box b_i. Next, the same procedure is performed where states i and j have exchanged places and the state i' is found. The matrix element between states i and j is then simply approximated as $\mathscr{M}_{ij,\mu} = \left(\mathscr{M}_{ij',\mu} + \mathscr{M}_{i'j,\mu}\right)/2$. Although this procedure is simple, it requires a detailed explanation to avoid any ambiguity in the description. This procedure produces the same statistical aspects of $\mathscr{M}_{ij,\mu}$ in the system as in the periodic system consisting of only b_i or b_j.

9 Calculation of equivalent conductance at length scales L_3 and L_4

The equivalent conductance of the conductor network at length scale L_3 is found by solving the linear equations for the potentials of nodes in the circuit. Periodic boundary conditions are applied

in two directions (say y and z) and the voltage is applied in third direction (say x). This is achieved by periodically replicating the supercell (of the size $L_x = L_y = L_z = L$) to an infinite system and applying the conditions: $V_i - V_j = 0$ if $\mathbf{r}_i - \mathbf{r}_j = \pm L\mathbf{e}_y$ or $\mathbf{r}_i - \mathbf{r}_j = \pm L\mathbf{e}_z$ and $V_i - V_j = \pm U$ if $\mathbf{r}_i - \mathbf{r}_j = \pm L\mathbf{e}_x$ (where $\mathbf{r}_i$ is the position of node i, V_i its potential and $\mathbf{e}_x$, $\mathbf{e}_y$, $\mathbf{e}_z$ the unit vectors in the three directions). The current conservation equations for the potentials of the nodes read

$$V_i \sum_j G_{ij} - \sum_j V_j G_{ji} = 0.$$

A closed system of equations is formed by writing the previous equation for all nodes i in a supercell except for one whose potential is set to zero. The current I_x through a plane perpendicular to the x direction is then calculated and the equivalent conductance is found as $G_x = I_x/U$. The mobility in $x-$direction is then given by $\mu_x = G_x/(neL)$, where n is the concentration of carriers. Since both the conductance in the small carrier density limit and the concentration depend linearly on the total number of carriers, the mobility is independent of the carrier density.

The continuum system at length scale L_4 is discretized for the numerical simulation by the simplest possible method where a single node is assigned to the center of each of the boxes, which transforms the continuum into a discrete conductor network with $k_2 \times k_2 \times k_2$ nodes. By comparing the results with more detailed discretization schemes, it has been checked that such a simplification does not change the final mobility by more than 30%. The equivalent conductance of the conductor network is then found in the same manner as described for the network at length scale L_3.

References

(1) http://hpcrd.lbl.gov/∼linwang/PEtot/PEtot.html.

(2) Vukmirović, N.; Wang, L.-W. *J. Chem. Phys.* **2008**, *128*, 121102.

(3) Vukmirović, N.; Wang, L.-W. *J. Phys. Chem. B* **2009**, *113*, 409–415.

(4) Hwang, M. J.; Stockfisch, T. P.; Hagler, A. T. *J. Am. Chem. Soc.* **1994**, *116*, 2515–2525.

(5) Maple, J. R.; Hwang, M.-J.; Stockfisch, T. P.; Dinur, U.; Waldman, M.; Ewig, C. S.; Hagler, A. T. *J. Comp. Chem.* **1994**, *15*, 162–182.

(6) http://lammps.sandia.gov.

(7) Plimpton, S. J. *J. Comp. Phys.* **1995**, *117*, 1–19.

(8) Mardalen, J.; Samuelsen, E. J.; Gautun, O. R.; Carlsen, P. H. *Solid State Comm*, **1991**, *77*, 337–339.

(9) Mardalen, J.; Samuelsen, E. J.; Gautun, O. R.; Carlsen, P. H. *Synth. Met.* **1992**, *48*, 363–380.

(10) Marchant, S.; Foot, P. J. S. *Polymer* **1997**, *38*, 1749–1751.

(11) Kim, S.-S.; Na, S.-I.; Jo, J.; Tae, G.; Kim, D.-Y. *Adv. Mater.* **2007**, *19*, 4410–4415.

(12) Wang, L.-W.; Zunger, A. *J. Chem. Phys.* **1994**, *100*, 2394–2397.

(13) Canning, A.; Wang, L. W.; Williamson, A.; Zunger, A. *J. Comp. Phys.* **2000**, *160*, 29–41.

(14) Meisel, K. D.; Vocks, H.; Bobbert, P. A. *Phys. Rev. B* **2005**, *71*, 205206.

(15) Zade, S. S.; Bendikov, M. *Chem. Eur. J.* **2008**, *14*, 6734–6741.

(16) Bylaska, E. J.; de Jong, W. A.; Govind, N.; Kowalski, K.; Straatsma, T. P.; Valiev, M.; Wang, D.; Apra, E.; Windus, T. L.; Hammond, J.; Nichols, P.; Hirata, S.; Hackler, M. T.; Zhao, Y.; Fan, P.-D.; Harrison, R. J.; Dupuis, M.; Smith, D. M. A.; Nieplocha, J.; Tipparaju, V.; Krishnan, M.; Wu, Q.; Voorhis, T. V.; Auer, A. A.; Nooijen, M.; Brown, E.; Cisneros, G.; Fann, G. I.; Fruchtl, H.; Garza, J.; Hirao, K.; Kendall, R.; Nichols, J. A.; Tsemekhman, K.; Wolinski, K.; Anchell, J.; Bernholdt, D.; Borowski, P.; Clark, T.; Clerc, D.; Dachsel, H.; Deegan, M.; Dyall, K.; Elwood, D.; Glendening, E.; Gutowski, M.; Hess, A.; Jaffe, J.; Johnson, B.; Ju, J.; Kobayashi, R.; Kutteh, R.; Lin, Z.; Littlefield, R.; Long, X.; Meng, B.; Nakajima, T.; Niu, S.; Pollack, L.; Rosing, M.; Sandrone, G.; Stave, M.; Taylor, H.; Thomas, G.; van Lenthe, J.; Wong, A.; ; Zhang, Z. *NWChem, A Computational*

Chemistry Package for Parallel Computers, Version 5.1; Pacific Northwest National Laboratory, Richland, Washington 99352-0999, USA, 2007.